Synthesis, characterization and thermochemistry of a Pb-jarosite

F.L. Forray [a,1], A.M.L. Smith [b], C. Drouet [c], A. Navrotsky [a,*], K. Wright [d], K.A. Hudson-Edwards [e], W.E. Dubbin [f]

[a] *Peter A. Rock Thermochemistry Laboratory and NEAT ORU, University of California at Davis, 1 Shields Avenue, Davis, CA 95616, USA*
[b] *Davy Faraday Research Laboratory, The Royal Institution of Great Britain, 21 Albemarle Street, London W1S 4BS, UK*
[c] *CIRIMAT Carnot Institute, University of Toulouse, CNRS/INPT/UPS, ENSIACET, 118 route de Narbonne, 31077 Toulouse Cedex 04, France*
[d] *Nanochemistry Research Institute, Department of Applied Chemistry, Curtin University of Technology, G.P.O. Box U1987, Perth, WA 6845, Australia*
[e] *Research School of Earth Sciences at UCL-Birkbeck, Birkbeck, University of London, Malet Street, London WC1E 7HX, UK*
[f] *Department of Mineralogy, The Natural History Museum, Cromwell Road, London SW7 5BD, UK*

Abstract

The enthalpy of formation from the elements of a well-characterized synthetic Pb-jarosite sample corresponding to the chemical formula $(H_3O)_{0.74}Pb_{0.13}Fe_{2.92}(SO_4)_2(OH)_{5.76}(H_2O)_{0.24}$ was measured by high temperature oxide melt solution calorimetry. This value ($\Delta H^\circ_f = -3695.9 \pm 9.7$ kJ/mol) is the first direct measurement of the heat of formation for a lead-containing jarosite. Comparison to the thermochemical properties of hydronium jarosite and plumbojarosite end-members strongly suggests the existence of a negative enthalpy of mixing possibly related to the nonrandom distribution of Pb^{2+} ions within the jarosite structure. Based on these considerations, the following thermodynamic data are proposed as the recommended values for the enthalpy of formation from the elements of the ideal stoichiometric plumbojarosite $Pb_{0.5}Fe_3(SO_4)_2(OH)_6$: $\Delta G^\circ_f = -3118.1 \pm 4.6$ kJ/mol, $\Delta H^\circ_f = -3603.6 \pm 4.6$ kJ/mol and $S^\circ = 376.6 \pm 4.5$ J/(mol K). These data should prove helpful for the calculation of phase diagrams of the Pb–Fe–SO_4–H_2O system and for estimating the solubility product of pure plumbojarosite. For illustration, the evolution of the estimated solubility product of ideal plumbojarosite as a function of temperature in the range 5–45 °C was computed (Log(K_{sp}) ranging from −24.3 to −26.2). An Eh–pH diagram is also presented.

Corresponding author. Address: Peter A. Rock Thermochemistry Laboratory and NEAT ORU, University of California at Davis, 4415 Chem Annex, 1 Shields Avenue, Davis, CA 95616, USA. Tel.: +1 530 752 3292; fax: +1 530 752 9307.
E-mail address: anavrotsky@ucdavis.edu (A. Navrotsky).
[1] Present address: Department of Geology, Babeş-Bolyai University, M. Kogălniceanu 1, 400084 Cluj-Napoca, Romania.

1. INTRODUCTION

Lead jarosite is a member of the jarosite family $AFe_3(SO_4)_2(OH)_6$, which belongs to the alunite supergroup of minerals. The end-member plumbojarosite, $Pb_{0.5}Fe_3(SO_4)_2(OH)_6$, occurs in Pb-bearing soils (Özacar et al., 2000) and in areas of sulfide mineral oxidation, including acid rock and acid mine drainages (Knopf, 1915; Hudson-Edwards et al., 1999; Dutrizac and Jambor, 2000; Hochella et al., 2005). Plumbojarosite is also formed in some hydrometallurgical processes (Dutrizac, 1991; Patiño et al., 1994; Dutrizac and Jambor, 2000).

The 'A' sites in jarosite minerals are commonly occupied by alkali ions such as K^+ or Na^+, but numerous substitutions have been reported, reflecting the flexibility of the jarosite structure toward ion size and charge accommodation (Hendricks, 1937). This feature makes jarosite-like minerals especially suitable for trapping unwanted, potentially toxic metallic elements in the environment. Numerous studies have thus been dedicated to the incorporation of both trivalent and hexavalent chromium into the jarosite structure, leading to $KCr_3(SO_4)_2(OH)_6$ (Lengauer et al.,

1994) and $KFe_3(CrO_4)_2(OH)_6$ (Powers et al., 1975; Baron and Palmer, 1996b, 2002; Drouet et al., 2003) respectively, but other elements have also been investigated, including cadmium (Dutrizac et al., 1996), arsenic (Dutrizac and Jambor, 1987), gallium (Dutrizac and Chen, 2000), and mercury (Dutrizac and Chen, 1981). In many cases, departure from stoichiometry has been reported for jarosite and alunite samples, and has been related to the substitution of hydronium ions in 'A' sites and to the presence of iron/aluminum vacancies (Hendricks, 1937; Kubisz, 1970), where charge neutrality is ensured by the protonation of some hydroxyl groups, giving rise to an equivalent number of structural water molecules.

Despite the obvious interest in the precipitation of jarosite-like phases to trap Pb^{2+} ions from contaminated sites and in metallurgy, very few data are available in the literature on the thermodynamics or solubility of such lead-containing jarosites (Kashkay et al., 1975; Smith et al., 2006). Such data are required for thermodynamic calculations involving these phases, for example to establish phase diagrams, to compute equilibria among the solid phases formed and the surrounding aqueous solution, and to estimate dissolution products for solid solutions. In this study, high temperature oxide melt solution calorimetry was used to measure the heat of formation of a well-characterized Pb-containing jarosite sample. We then are able to draw conclusions concerning the thermochemistry of the hydronium jarosite–plumbojarosite solid solution (including enthalpies of mixing) as well as of the ideal plumbojarosite end-member itself. We finally evaluate, as a first approximation, the solubility product of this solid solution and present an Eh–pH diagram for part of the S–Fc–Pb–H_2O system.

2. EXPERIMENTAL

2.1. Synthesis and characterization

This work was carried out on a lead-containing jarosite (Pb-jarosite) compound prepared using the synthesis protocol described in a previous paper (Smith et al., 2006), and summarized briefly here. We followed the methods of Dutrizac and Kaiman (1976), Dutrizac et al. (1980), and Jambor and Dutrizac (1983), and produced a 1 L solution of 0.054 M $Fe_2(SO_4)_3{\cdot}5H_2O$ and 0.01 M H_2SO_4, which was heated in a sand bath to 95 °C, then added 200 mL of 0.03 M $Pb(NO_3)_2$, with stirring, at a rate of 6 mL h^{-1}. Once all the $Pb(NO_3)_2$ had been added, the precipitate was stirred (400 rpm) for a further 5 h, after which it was allowed to settle and the residual supernatant solution decanted. The precipitate was then thoroughly washed with ultrapure water (18 MΩ cm^{-1}) and dried at 110 °C for 24 h.

The synthetic Pb-jarosite was initially characterized by X-ray diffraction (XRD), quantitative wet chemistry, scanning electron microscopy (SEM), N_2 BET surface area analysis (Brunauer et al., 1938) and Fourier transform infrared spectroscopy (FTIR), and the main results were described in a previous report (Smith et al., 2006).

In addition to the previously reported characterization, additional data were obtained using thermogravimetry (TG) and differential thermal analysis (DTA) conducted simultaneously on a Remetric STA 1500H thermobalance. The synthetic Pb-jarosite sample (10.590 mg) was heated from 25 to 1100 °C at 10 °C min^{-1}, under an atmosphere of argon introduced at a rate of 30 mL min^{-1}. X-ray diffraction analyses were also performed after heating the Pb-jarosite sample under argon to various relevant temperatures selected from analysis of the TG–DTA profiles. The powder XRD patterns were collected in Bragg–Brentano reflection geometry on a Siemens D500 diffractometer operated at 40 kV and 40 mA at 25 °C. Cu Kα radiation ($\lambda = 1.54056$ Å) was used in conjunction with a secondary graphite monochromator and a scintillation counter. The divergence slit was 1° and the receiving slit 0.05°. The samples were mounted on a Bruker zero background silicon (510) sample holder. The initial and final 2θ angles were 10° and 70°, respectively. The step size was 0.020° 2θ and the measuring time was 18 s per step.

2.2. Calorimetry

Oxide melt drop solution calorimetry was run at 700 °C (973 K) using a custom-built Tian-Calvet twin calorimeter, and sodium molybdate ($3Na_2O{\cdot}4MoO_3$) solvent. A detailed description of the technique can be found elsewhere (Navrotsky, 1977, 1997; Drouet and Navrotsky, 2003). Pellets of the sample (5–15 mg) were dropped into a platinum crucible containing the solvent, located in the hot zone of the calorimeter. The end of the reaction was judged by the return of the calorimetric signal to its initial value. The final state in these calorimetric experiments is a dilute solution in $3Na_2O{\cdot}4MoO_3$ of the sulfates of Pb^{2+} and Fe^{3+} (as ions in the melt) and gaseous H_2O, all at 700 °C. Previous studies on simple sulfate and jarosite phases have shown that all the sulfur is retained in the melt rather than emitted as a gas (Majzlan et al., 2002; Drouet and Navrotsky, 2003). During our experiments, O_2 gas was flushed through the space above the melt (~35 mL/min) and bubbled through the solvent (~5 mL/min) to maintain oxidizing conditions, stir the melt, and remove the evolved H_2O vapor.

3. RESULTS AND DISCUSSION

3.1. Physico-chemical characterization

3.1.1. X-ray diffraction, elemental analysis, FTIR, SEM and BET

For the sake of completeness, the main results of previous characterization (Smith et al., 2006) are reviewed here.

The synthesis procedure was found to produce a yellow precipitate with Munsell color 10YR 6.5/7. The powder X-ray diffraction pattern matched that of the International Centre for Diffraction Data Powder Diffraction File for synthetic plumbojarosite (end-member Pb-jarosite; ICDD PDF 39-1353) (see Fig. 1 of Smith et al., 2006). No additional peaks were detected, suggesting that no other compounds were present at detectable levels. The calculated lattice parameters of the synthetic Pb-jarosite were $a_0 = 7.3347(7)$ Å and $c_0 = 16.9700(5)$ Å. While this a_0 is similar to that of the ICDD PDF file (7.335(1) Å), the c_0

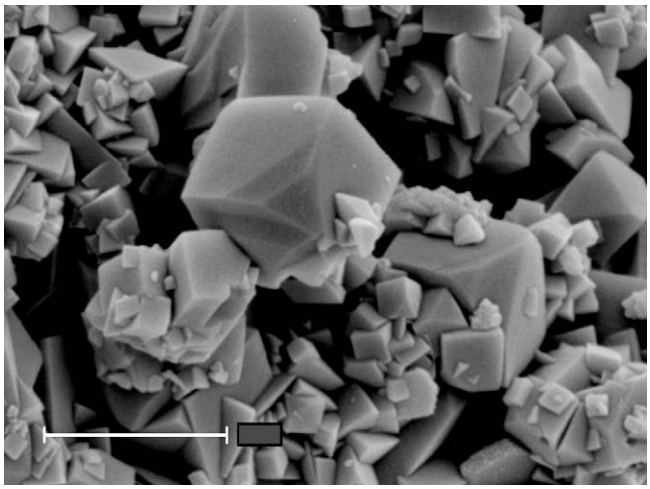

Fig. 1. Scanning electron microscope (SEM) images of synthetic Pb-jarosite. Scale bar equals 1 μm. The image was taken at 35,000× magnification, spot size 3.0, and 5 kV accelerating voltage.

is one-half of the corresponding ICDD value (33.850(8) Å). This discrepancy is attributed to the better fit (χ^2 values) achieved using a single, rather than a doubled, unit cell, and to the lack of superlattice XRD reflections (which would indicate a doubled unit cell) in the diffraction pattern for the synthetic Pb-jarosite (see Fig. 1 of Smith et al., 2006), although such doubling has been seen in natural samples (Dutrizac and Jambor, 2000).

The formula of the synthetic Pb-jarosite used in this work, calculated using the modified formula of Kubisz (1970), was found to be $Pb_{0.13}(H_3O)_{0.74}Fe_{2.92}(SO_4)_2(OH)_{5.76}(H_2O)_{0.24}$. Thus this synthetic lead-bearing jarosite differs noticeably from the ideal stoichiometric plumbojarosite end-member $Pb_{0.5}Fe_3(SO_4)_2(OH)_6$ despite highly similar XRD patterns. This compound is actually an intermediate member of the hydronium–plumbojarosite solid solution, and exhibits a nonstoichiometry in the B-sites of the jarosite structure pointed out by the iron content of 2.92 rather than 3 per unit formula. The presence of a significant amount of hydronium ions can most probably be related to the low pH used here for jarosite synthesis, leading to a high activity H_3O^+ ions. Such a substantial level of hydronium substitution for lead was likewise evidenced by Ripmeester et al. (1986). Also, the nonstoichiometry is customary for apatites prepared from wet chemistry at moderate temperatures and probably also applies to some other early studies (e.g. Kashkay et al., 1975) dealing with the precipitation of jarosites at room temperature and for which only limited characterization techniques were accessible.

The apparent difficulty to prepare by soft chemistry (chimie douce, meaning synthesis under at moderate temperature and pressure conditions, generally involving aqueous or other solvents) a pure plumbojarosite sample might find crystallographic explanation. Indeed, in the lead-hydronium jarosite solid solution, as the lead content increases a structural change (doubling of the *c*-axis parameter) was reported in the literature. Mumme and Scott (1966) suggested that this doubling occurred only if the mineral stoichiometry was very close to the ideal end-member formula. However, according to Jambor and Dutrizac (1983), less then a third of the A-site of the jarosite structure needs to be filled by Pb^{2+} in order to attain the ~35 Å *c*-axis parameter. At this lead concentration, the H_3O^+ content reaches 0.33 per unit formula. In any case, the development of superstructure might create a miscibility gap in the solid solution between plumbojarosite and hydronium jarosite. Jambor and Dutrizac (1983) also suggested, in a similar context, the existence of a structural discontinuity for beaverite–plumbojarosite solid solution due to the doubled *c*-axis of the plumbojarosite compared to beaverite, but additional well documented work is needed to clarify these aspects.

In the following, the Pb-jarosite sample examined in the present work will be referred to as "ns-Pb0.13-jar" standing for "nonstoichiometric $Pb_{0.13}$-hydronium jarosite" where the amount of hydronium can be evaluated by electroneutrality based on the relation $n_{H3O+} = 1–2x$ where "*x*" stands for the lead content.

The FTIR spectrum of this sample (not shown here, see Fig. 3 of Smith et al., 2006) is similar to those previously reported for jarosites of other compositions (Powers et al., 1975; Serna et al., 1986; Baron and Palmer, 1996a; Drouet and Navrotsky, 2003), thus confirming the jarosite phase identity of this compound.

SEM observations recently taken on this sample indicate a rhombohedral (pseudocubic) morphology, which is characteristic of many lead-bearing jarosite precipitates (Fig. 1) (Dutrizac and Chen, 2003), and involve intergrown crystals with diameters ranging from 0.5 to 2 μm. In contrast, lead-containing jarosites prepared in an autoclave at elevated temperatures exhibit a euhedral crystal habit (Dutrizac et al., 1980).

The N_2 BET specific surface area for ns-Pb0.13-jar is $1.03 \pm 0.023\ m^2\ g^{-1}$. Currently, there are no published data on the surface area of synthetic Pb-jarosites, but surface area studies on some monovalent cation jarosites were reported and areas were found to range from 0.5 to $4.0\ m^2\ g^{-1}$ (Sasaki and Konno, 2000). Thus, when com-

pared to such other jarosites, the sample ns-Pb0.13-jar is relatively coarse-grained, well crystallized and not of nanoscale dimensions. Its relatively small surface area indicates that surface effects can be neglected in thermodynamic considerations.

3.1.2. Thermal analyses

The total weight loss over the temperature range 25–1100 °C is 47.5% (Fig. 2a). The TG curve shows that the weight loss occurs over three principal temperature intervals: (1) 15% weight loss between 150 and 500 °C, (2) 31% weight loss between 500 and 1000 °C, and (3) 1.5% weight loss between 1000 and 1100 °C. The DTA curve indicates both a strong endotherm at 662 °C and a weak one at 428 °C. A series of small endothermic peaks are also present between 150 and 300 °C, and are similar to the peaks reported by Özacar et al. (2000) for a natural specimen of plumbojarosite.

The 15% weight loss between 150 and 500 °C can be attributed to two specific mechanisms. The first is related to the removal of the "additional water", meaning protonated OH^- ions, that form water molecules are still located in OH sites of the jarosite structure (where such protonation is thought to accommodate the lack of positive charges due to iron and A-site cation vacancies). This weight loss coincides with the series of small endothermic peaks in the DTA between 150 and 300 °C (Kubisz, 1971; Baron and Palmer, 1996a; Drouet and Navrotsky, 2003). The theoretical weight loss attributed to this loss of "additional water", calculated from the stoichiometry of the sample, is 0.86 wt.%. The second more intense process, which contributes to the main part of the 15% weight loss, is the breakdown of the jarosite structure through its dehydroxylation. XRD analysis performed on the sample retrieved after treatment at 490 °C suggests that $Fe_2(SO_4)_3$ is the most abundant crystallized phase remaining after the re-

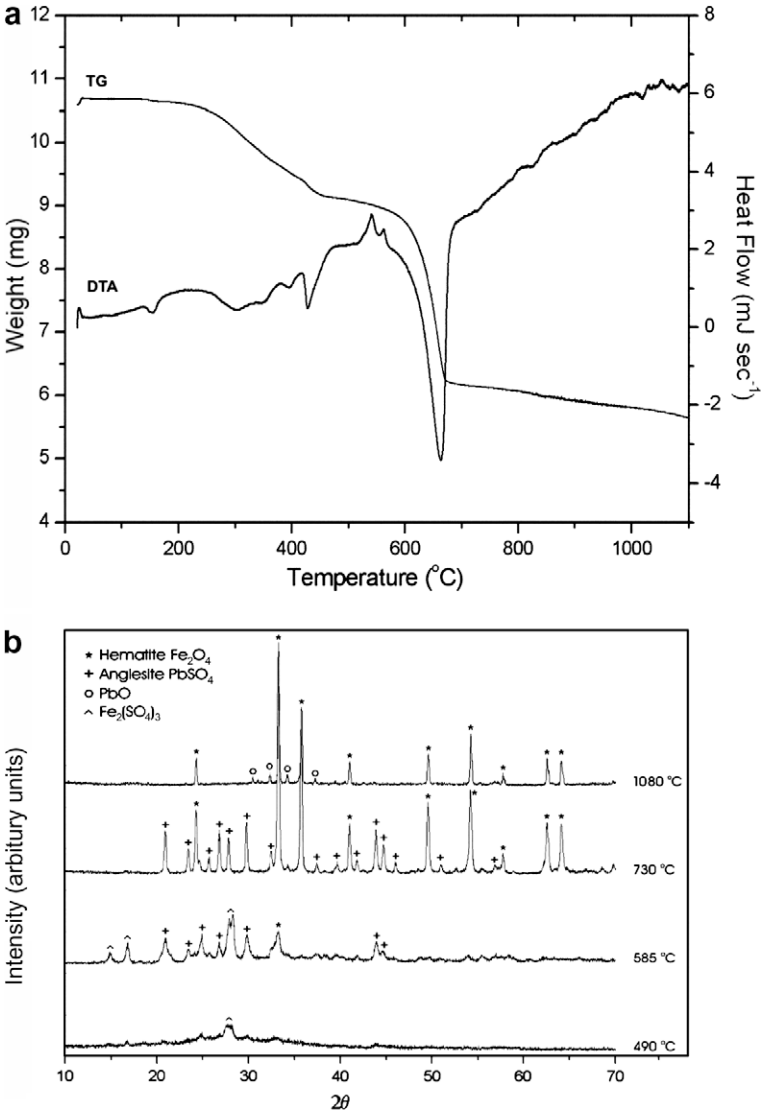

Fig. 2. (a) TG–DTA profiles of synthetic Pb-jarosite (b) Powder XRD patterns for the thermal decomposition of synthetic Pb-jarosite under argon at 490, 585, 730, and 1080 °C (Cu Kα radiation, $\lambda = 1.54056$ Å).

moval of all the structural water (Fig. 2b). The dehydroxylation reaction for the ns-Pb0.13-jar sample can be summarized by the reaction:

$$Pb_{0.13}(H_3O)_{0.74}Fe_{2.92}(SO_4)_2(OH)_{5.76} \rightarrow 0.13PbSO_4 + 0.623Fe_2(SO_4)_3 + 0.837Fe_2O_3 + 3.99H_2O_{(g)} \quad (1)$$

In this case, the theoretical weight loss based on stoichiometry is 14.4 wt.%. The sum of these two weight losses is 15.26 wt.% which compares well with the 15 wt.% overall weight loss observed by TG.

Eq. (1) indicates the formation of Fe_2O_3 upon dehydroxylation. It is worth mentioning the presence of a small exothermic peak in the DTA curve, observed at 541 °C, which finds no corresponding weight loss peak on the TG curve. This peak can probably be associated with the crystallization of hematite (α-Fe_2O_3) (Fig. 2b) as already reported (Drouet and Navrotsky, 2003). It can be also be noted that the decomposition of this ns-Pb0.13-jar sample does not produce any anhydrous double sulfates, while potassium jarosite ($KFe(SO_4)_2(OH)_6$) decomposes to form yavapaiite ($KFe(SO_4)_2$) (Forray et al., 2005).

The second and most significant weight loss observed by TG analysis (31%) occurs between 500 and 1000 °C, and coincides with the most intense endothermic peak in the DTA curve at 662 °C. This loss can be attributed to the thermal decomposition of $Fe_2(SO_4)_3$ into crystalline α-Fe_2O_3 and the release of sulfur-containing gas (Fig. 2b) (Özacar et al., 2000). The theoretical calculated weight loss for this decomposition is 30%, and the reaction can be expressed as follows:

$$0.623Fe_2(SO_4)_3 \rightarrow 0.623Fe_2O_3 + 1.869SO_{3(g)} \quad (2)$$

Note that the gas actually released may contain a mixture of sulfur species, but reaction (2) expresses the overall stoichiometry. Again, a good fit between the experimental data and the evaluated chemical composition of the starting sample was found.

The final weight loss (1.5%) occurs between 1000 and 1100 °C. Özacar et al. (2000) proposed that this weight loss could be associated with the breakdown of anglesite ($PbSO_4$) into lead oxide (theoretical weight loss: 2%) and this has indeed been confirmed here by XRD analysis of the residual solid retrieved after heating to 1080 °C (Fig. 2b). The relevant reaction is:

$$0.13PbSO_4 \rightarrow 0.13PbO + 0.13SO_{3(g)} \quad (3)$$

The differences in decomposition temperatures between hydronium jarosite (Majzlan et al., 2004), sample ns-Pb0.13-jar, and end-member plumbojarosite prepared by Frost et al. (2005) suggest that an increase in Pb content in jarosite lowers the decomposition temperature of the $Fe_2(SO_4)_3$ phase. This might then suggest the presence of some Pb^{2+} ions within this iron sulfate as a solid solution.

3.2. Calorimetry

The enthalpy of formation from the elements, ΔH°_f, of ns-Pb0.13-jar was determined in the present work from its enthalpy of drop solution, ΔH_{ds}, in sodium molybdate at 700 °C ($\Delta H_{ds} = 477.1 \pm 5.1$ kJ/mol), using the thermodynamic cycle given in Table 1. This cycle involves the enthalpy of drop solution of another lead-containing compound, namely reagent grade lead carbonate $PbCO_3$, also measured here ($\Delta H_{ds} = 101.4 \pm 0.8$ kJ/mol), as well as other thermodynamic data taken from the literature (Robie and Hemingway, 1995; Bale et al., 2002; Majzlan et al., 2002;

Table 1
Thermodynamic cycle for the determination of ΔH°_f from the elements.

Reaction[a]	ΔH (kJ/mol)[b]
(1) $Pb_x(H_3O)_{1-2x}Fe_{3-y}(SO_4)_2(OH)_{6-3y}(H_2O)_{3y}$(s, 298) → x PbO (soln, 973) + $(3-y)/2$ Fe_2O_3 (soln, 973) + 2 SO_3 (soln, 973) + $(9-6x+3y)/2$ H_2O (g, 973)	ΔH_{ds} (Pb-jarosite)
(2) $PbCO_3$ (s, 298) → PbO (soln, 973) + CO_2 (g, 973)	ΔH_{ds} ($PbCO_3$)
(3) Pb (s, 298) + C (s, 298) + 3/2 O_2 (g, 298) → $PbCO_3$ (s, 298)	ΔH°_f ($PbCO_3$)
(4) CO_2 (g, 298) → CO_2 (g, 973)	ΔH_{hc} ($CO_{2(g)}$)
(5) C (s, 298) + O_2 (g, 298) → CO_2 (g, 298)	ΔH°_f ($CO_{2(g)}$)
(6) α-Fe_2O_3 (s, 298) → Fe_2O_3 (soln, 973)	ΔH_{ds} (α-Fe_2O_3)
(7) 2 Fe (s, 298) + 3/2 O_2 (g, 298) → α-Fe_2O_3 (s, 298)	ΔH°_f (Fe_2O_3)
(8) SO_3 (g, 298) → SO_3 (soln, 973)	ΔH_{ds} ($SO_{3(g)}$)[c]
(9) S (s, 298) + 3/2 O_2 (g, 298) → SO_3 (g, 298)	ΔH°_f ($SO_{3(g)}$)
(10) H_2O (g, 298) → H_2O (g, 973)	ΔH_{hc} ($H_2O_{(g)}$)
(11) H_2 (g, 298) + 1/2 O_2 (g, 298) → H_2O (g, 298)	ΔH°_f ($H_2O_{(g)}$)
Formation of Pb-jarosite:	
(12) x Pb (s, 298) + $(3-y)$ Fe (s, 298) + 2 S (s, 298) + $(15-2x)/2$ O_2 (g, 298) + $(9-6x+3y)/2$ H_2 (g, 298) → $Pb_x(H_3O)_{1-2x}Fe_{3-y}(SO_4)_2(OH)_{6-3y}(H_2O)_{3y}$(s, 298)	ΔH°_f (Pb-jarosite)
ΔH°_f (Pb-jarosite) = $-\Delta H_1 + x\,\Delta H_2 + x\,\Delta H_3 - x\,\Delta H_4 - x\,\Delta H_5 + (3-y)/2\,\Delta H_6 + (3-y)/2\,\Delta H_7 + 2\,\Delta H_8 + 2\,\Delta H_9 + (9-6x+3y)/2\,\Delta H_{10} + (9-6x+3y)/2\,\Delta H_{11}$	

[a] "s", "g" and "soln" are for "solid", "gas","in solution" (in sodium molybdate) and the temperature in Kelvin.
[b] ΔH_{ds}, ΔH°_f and ΔH_{hc} are, respectively, the drop solution enthalpy, standard enthalpy of formation and heat content.
[c] ΔH_{ds} ($SO_{3(g)}$) as determined by Majzlan et al. (2002).

Drouet and Navrotsky, 2003) and listed in Table 2. The application of this thermodynamic cycle then leads, for sample ns-Pb0.13-jar, to the heat of formation from the elements of $\Delta H^\circ_f = -3695.9 \pm 9.7$ kJ/mol.

Since the enthalpy contribution to the Gibbs free energy is, for such multiple oxide/hydroxide compounds, by far the preponderant term (as opposed to any entropic term, see for example Drouet and Navrotsky, 2003), conclusions about relative thermodynamic stabilities can be drawn, in a first approach, by comparing the heats of formation of the various series of jarosites. In particular, this value ($\Delta H^\circ_f = -3695.9 \pm 9.7$ kJ/mol) is found to be close to the one ($\Delta H^\circ_f = -3694.5 \pm 4.6$ kJ/mol) reported recently by Majzlan et al. (2004) on a nonstoichiometric hydronium jarosite sample exhibiting a very similar level of nonstoichiometry. In contrast, the value measured for ns-Pb0.13-jar is less exothermic than the heats of formation reported for nonstoichiometric potassium jarosites or sodium jarosites, which are in the range −3725 to −3805 kJ/mol (Drouet and Navrotsky, 2003). These findings indicate that this sample has a thermodynamic stability close to that of nonstoichiometric (Pb-free) hydronium jarosite, since the incorporation of 0.13 mol of Pb^{2+} per mole of hydronium jarosite does not lead to a noticeable change in the corresponding heat of formation. This stability is noticeably lower than that of the K- or Na-jarosite series.

Due to the lack of thermodynamic data concerning lead-containing jarosites, it is not possible to compare directly this ΔH°_f value to other experimental determinations. It is then of interest to estimate the enthalpy of formation of the plumbojarosite end-member, based on some reported data. Since the enthalpies of formation for ns-Pb0.13-jar and hydronium jarosite are for nonstoichiometric jarosites (with an Fe content close to 2.92 rather than 3), the possibility to estimate the heat of formation ΔH°_f(ns-plumbojar) of the plumbojarosite nonstoichiometric analog (also corresponding to an iron content close to 2.92) was explored first.

A possible way to evaluate this value is to use the equation defining the Gibbs free energy, which can be rewritten as $\Delta H^\circ_f = \Delta G^\circ_f + T \cdot \Delta S^\circ_f$. Kashkay et al. (1975) have reported the value $\Delta G^\circ_f = -3023.0 \pm 2.0$ kJ/mol for the free energy of formation of a lead-jarosite sample prepared by wet chemistry (coprecipitation from sulfate salts) at room temperature. Although only very limited characterization data were given by these authors, such conditions of formation are known to generally lead to nonstoichiometric jarosites and seldom to stoichiometric end-members (e.g. Dutrizac and Jambor, 1985), thus a comparison with the ns-Pb0.13-jar sample prepared here appears reasonable.

It has to be noted that Gaboreau and Vieillard (2004) recalculated this ΔG°_f value based on the original experimental data from Kashkay et al. (1975) but using more recent data for the free energy of aqueous ions, leading to $\Delta G^\circ_f = -3037.2 \pm 4.0$ kJ/mol. This value is the one considered in the following discussion, and its uncertainty was

Table 2
Thermodynamic data used in this work.

Compound	ΔH_{ds} (kJ/mol)	ΔH_{hc} (kJ/mol)	$\Delta H^\circ_{f,298k}$ (kJ/mol)	S°_{298k} (J/(mol K))	$\Delta G^\circ_{f,298k}$ (kJ/mol)
$PbCO_{3(s)}$	101.4 ± 0.8 (7)[a]	–	-699.2 ± 1.2[b]		
α-$Fe_2O_{3(s)}$	95.0 ± 1.8[c]	–	-826.2 ± 1.3[b]		
$SO_{3(g)}$	-205.8 ± 3.7[d]	–	-395.7 ± 0.7[b]		
$CO_{2(g)}$	–	31.94 ± 0.0[e]	-393.5 ± 0.1[b]		
$H_2O_{(g)}$	–	24.89 ± 0.0[e]	-241.8 ± 0.0[b]		
$Pb_{0.13}(H_3O)_{0.74}Fe_{2.92}(SO_4)_2(OH)_{5.76}(H_2O)_{0.24}$					
	477.1 ± 5.1 (6)[a]		-3695.9 ± 9.7[a]		
$Pb^{2+}{}_{(aq)}$	–	–	0.9 ± 0.3[b]	18.5 ± 1[b]	-24.2 ± 0.2[b]
$Fe^{3+}{}_{(aq)}$	–	–	-49.9 ± 5.0[b]	-280 ± 13[b]	-16.7 ± 2[b]
$SO_4{}^{2-}{}_{(aq)}$	–	–	-909.3 ± 0.4[b]	18.5 ± 0.4[b]	-744 ± 0.4[b]
$H_2O_{(l)}$	–	–	-285.8 ± 0.1[b]	70 ± 0.1[b]	-237.1 ± 0.1[b]
$Pb_{(s)}$	–	–	0	64.8 ± 0.5[b]	–
$Fe_{(s)}$	–	–	0	27.09 ± 0.13[b]	–
$S_{(s)}$	–	–	0	32.05 ± 0.05[b]	–
O_2(g)	–	–	0	205.15 ± 0.02[b]	–
H_2(g)	–	–	0	130.68 ± 0.02[b]	–
$PbO_{(s)}$	–	–	–	66.5 ± 0.2[b]	–
$K_2O_{(s)}$	–	–	–	94.1 ± 6.3[b]	–
$Na_2O_{(s)}$	–	–	–	75.3 ± 0.8[b]	–
K-jarosite	–	–	–	388.9[f]	–
Na-jarosite	–	–	–	382.4[f]	–

[a] This work. Parentheses are the numbers of experiments performed.
[b] Robie and Hemingway (1995).
[c] Drouet and Navrotsky (2003).
[d] Majzlan et al. (2002).
[e] FactSage 5.3, thermodynamic software and database, © Termfact, Bale et al. (2002).
[f] Stoffregen (1993).

recalculated from the uncertainties on the free energy of aqueous ions.

The absolute entropy for such a nonstoichiometric plumbojarosite S°(ns-plumbojar) can be estimated from the following solid state reactions involving either nonstoichiometric potassium jarosite $KFe_{2.92}(SO_4)_2(OH)_{5.76}(H_2O)_{0.24}$ or sodium jarosite $NaFe_{2.92}(SO_4)_2(OH)_{5.76}(H_2O)_{0.24}$:

$$Pb_{0.5}Fe_{2.92}(SO_4)_2(OH)_{5.76}(H_2O)_{0.24} + \frac{1}{2}K_2O \rightarrow KFe_{2.92}(SO_4)_2(OH)_{5.76}(H_2O)_{0.24} + \frac{1}{2}PbO \quad (4)$$

$$Pb_{0.5}Fe_{2.92}(SO_4)_2(OH)_{5.76}(H_2O)_{0.24} + \frac{1}{2}Na_2O \rightarrow NaFe_{2.92}(SO_4)_2(OH)_{5.76}(H_2O)_{0.24} + \frac{1}{2}PbO \quad (5)$$

It is reasonable to assume that the entropy change of these reactions (which involve only solid phases thus leading to negligible volume changes) is close to zero. Thus the value of S°(ns-plumbojar) can be derived from the entropies of K_2O, Na_2O and PbO (Robie and Hemingway, 1995), and of nonstoichiometric potassium jarosite and sodium jarosite. The latter two are not accessible in the literature. However, Majzlan et al. (2004) showed that the difference in absolute entropies between stoichiometric and nonstoichiometric hydronium jarosites was small (about 2.3%), which allows us to apply Eqs. (4) and (5) with the entropy values of stoichiometric K- and Na-jarosite end-members (Stoffregen, 1993).

The standard entropy for nonstoichiometric plumbojarosite found by applying Eqs. (4) and (5) is 375.1 ± 4.5 J/(mol K) and 378.0 ± 0.6 J/(mol K) respectively, leading to a reasonable average value of S°(ns-plumbojar) = 376.6 ± 4.5 J/(mol K). This value of S° then leads to an entropy change ΔS°_f(ns-plumbojar) = -1646.7 ± 4.5 J/(mol K), for the formation of this phase from the elements.

The above discussion suggests that, to a first approximation, the following values can be proposed for nonstoichiometric plumbojarosite (for iron contents close to 2.92): ΔG°_f(ns-plumbojar) = -3037.2 ± 4.0 kJ/mol and ΔS°_f(ns-plumbojar) = -1646.7 ± 4.5 J/(mol K). These values then lead, by applying the relation $\Delta H^\circ_f = \Delta G^\circ_f + T \cdot \Delta S^\circ_f$ at 298 K, to the heat of formation from the elements: ΔH°_f(ns-plumbojar) = -3527.9 ± 4.0 kJ/mol. This value is clearly less exothermic than the one reported for nonstoichiometric hydronium jarosite with a similar Fe content ($\Delta H^\circ_f = -3694.5 \pm 4.6$ kJ/mol, Majzlan et al., 2004) which underlines the lower stability of the nonstoichiometric plumbojarosite end-member. This point can probably explain the difficulty encountered by many authors for preparing Pb-jarosites with maximum Pb^{2+}/H_3O^+ substitution, at least when using room temperature wet chemical routes.

The above findings reveal two interesting conclusions which appear contradictory at first glance: (i) the incorporation of 0.13 Pb^{2+} into the hydronium jarosite structure does not lead to a significant change in the heat of formation of the related jarosite compound and (ii) on the other hand the heat of formation of nonstoichiometric plumbojarosite (free of hydronium ions) is noticeably less exothermic than that of the hydronium analog. These findings can however, be plausibly explained by the existence of a negative mixing enthalpy, as already observed in the case of other jarosite compounds (e.g. for chromate-sulfate substitutions in potassium jarosite, Drouet et al., 2003), thus unveiling a deviation from thermodynamic ideality.

For the nonstoichiometric solid solution considered here (Fe content close to 2.92), the enthalpy of mixing $\Delta H_{mix}(x)$ corresponding to a Pb content noted "x" can be defined as the enthalpy of the reaction forming 1 mol of solid solution member starting from the two corresponding nonstoichiometric end-members:

$$2xPb_{0.5}Fe_{2.92}(SO_4)_2(OH)_{5.76}(H_2O)_{0.24} + (1-2x) \times (H_3O)Fe_{2.92}(SO_4)_2(OH)_{5.76}(H_2O)_{0.24} \rightarrow Pb_x(H_3O)_{1-2x}Fe_{2.92}(SO_4)_2(OH)_{5.76}(H_2O)_{0.24} \quad (6)$$

with $\Delta H_{mix}(x) = \Delta H^\circ_f$(ns-Pb($x$)-jar) $- (2x)\cdot\Delta H^\circ_f$(ns-plumbojar) $- (1-2x)\cdot\Delta H^\circ_f$(ns-$H_3O$-jar). The application of this equation to $x = 0.13$, while considering the value -3694.5 ± 4.6 kJ/mol determined by Majzlan et al. (2004) for ΔH°_f(ns-H_3O-jar), leads to $\Delta H_{mix}(0.13) = -44.7 \pm 10.7$ kJ/mol. Despite a rather high propagated uncertainty, this finding points out a significant negative enthalpy of mixing. It can be related to the relative facility to incorporate some extent of Pb^{2+} in hydronium jarosite while the complete substitution is not favored considering the relative stabilities of the phases. Interestingly, this enthalpy of mixing appears more exothermic than for the sulfate-chromate jarosite solid solution (ranging between -25 and 0 kJ/mol, Drouet et al., 2003) where the nonrandom distribution of the chromate and sulfate groups was already suggested. Similarly here, the ordering of the Pb^{2+} ions within the A-site array (leading to a nonrandom positioning of the related cationic vacancies) in the jarosite structure is suggested, which can be related to the crystallographic considerations mentioned above.

The enthalpies of formation for the two nonstoichiometric end-members and the sample ns-Pb0.13-jar are shown in Fig. 3. On this figure, the deviation from thermodynamic ideality (i.e. nonzero mixing enthalpy) can be graphically witnessed by the difference between the curve (second-order polynomial) and the dotted straight line linking the two end-members (corresponding to the thermodynamically-ideal nonstoichiometric solid solution).

On Fig. 3, the enthalpy of formation of the ideal stoichiometric hydronium jarosite end-member, as reported by Majzlan et al. (2004), and the enthalpy of formation ΔH°_f(plumbojar) = -3603.6 ± 4.6 kJ/mol for the ideal stoichiometric plumbojarosite $Pb_{0.5}Fe_3(SO_4)_2(OH)_6$ was extrapolated and added to the graph. If the absolute entropy of this compound is considered to be close to that of the nonstoichiometric analog, as was found for hydronium jarosite, then the value S° = 376.6 ± 4.5 J/(mol K) may be regarded as a good approximation, which leads in turn to the entropy of formation from the elements: ΔS°_f(plumbojar) $\sim -1629.3 \pm 4.5$ J/(mol K).

Based on these considerations, the following thermodynamic data are probably to-date the best approximations

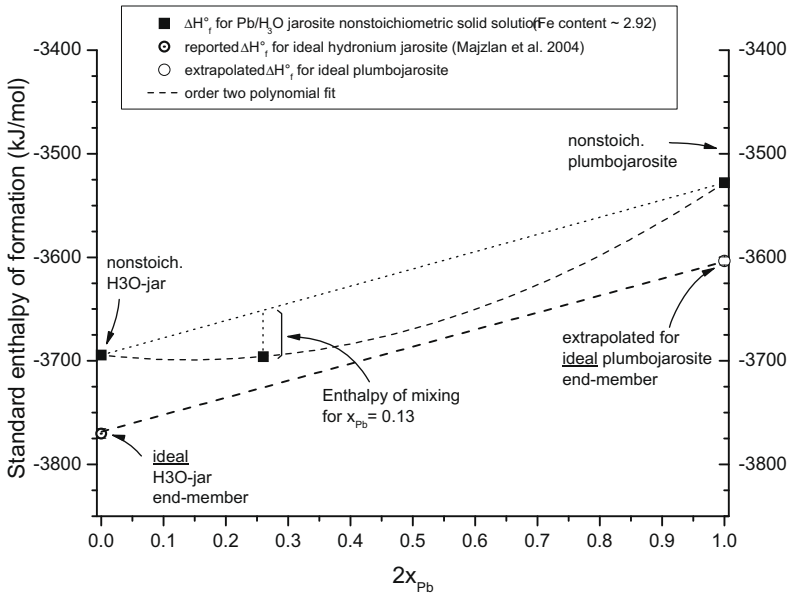

Fig. 3. Enthalpy of formation for the lead-hydronium jarosite solid solution and for ideal stoichiometric end-members, versus lead content.

for the formation of the ideal stoichiometric plumbojarosite $Pb_{0.5}Fe_3(SO_4)_2(OH)_6$: $\Delta G^\circ_f(\text{plumbojar}) = -3118.1 \pm 4.6$ kJ/mol, $\Delta H^\circ_f(\text{plumbojar}) = -3603.6 \pm 4.6$ kJ/mol and $S^\circ(\text{plumbojar}) \sim 376.6 \pm 4.5$ J/(mol K). These values should prove helpful for the establishment of phase diagrams of the Pb–Fe–SO_4–H_2O system or for the readjustment of existing diagrams.

Using our data on plumbojarosite and additional thermodynamic data for anglesite (Barin, 1993) and for galena (Barin, 1989), we calculated an Eh–pH diagram (Fig. 4). This diagram takes into account only these three mineral phases. Most frequently, plumbojarosite dissolution occur above a pH of 4 to 5 (Hochella et al., 1999). The diagram indicates that plumbojarosite is stable in conditions close to neutral pH. Decrease of the Pb concentration will make the plumbojarosite stable at higher pH. In the galena-arsenopyrite deposit of Baccu Locci in Sardinia (Italy), stream sediments and tailings have a pH of 7–8 and Eh of 0.4–0.6 V (Frau et al., 2009). In this environment Ardau et al. (2007) and Frau et al. (2007, 2009) identified plumbojarosite. This is reasonably consistent with our analysis.

The Eh–pH diagram also shows that in most environments galena alters to anglesite and anglesite to plumbojarosite and in only very narrow Eh–pH conditions does galena alter to plumbojarosite. The variation of the Pb concentration will influence the equilibrium between plumbojarosite and anglesite. There is field evidence of replacement of plumbojarosite by anglesite (Leybourne et al., 2006) and dissolution of anglesite and precipitation of plumbojarosite (Ostergren et al., 1999). This indicates

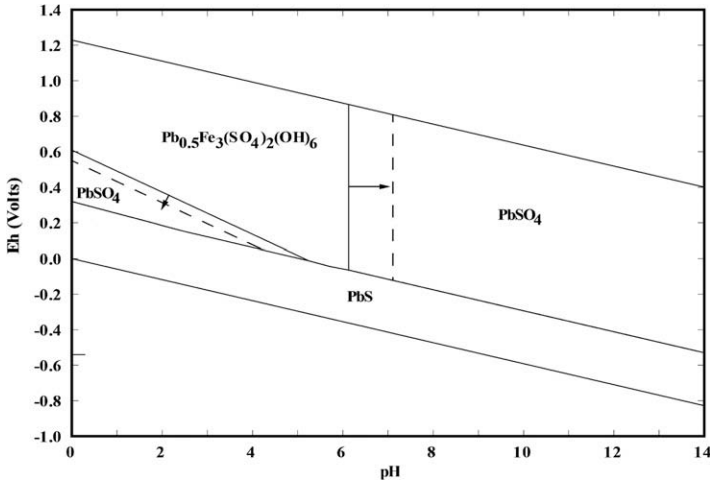

Fig. 4. Eh–pH diagram for part of the system S–O–Fe–Pb–H_2O at 25 °C. The assumed activities of dissolved species are 10^{-3} mol/L for S, Fe, and 10^{-6} mol/L (solid line) and 10^{-8} mol/L (doted line) for Pb. The arrows indicate the direction of shift of the boundaries for the two Pb concentrations.

Table 3
Estimated variation of the solubility product K_{sp} for ideal stoichiometric plumbojarosite versus temperature.

T (°C)	T (K)	$\Delta G^{\circ}_{f,dissolution}$ (kJ/mol)	Log(K_{sp})
5	278	129.5 ± 9.8	−24.3
15	288	137.0 ± 9.8	−24.9
25	298	145.3 ± 9.8	−25.5
35	308	152.0 ± 9.8	−25.8
45	318	159.5 ± 9.8	−26.2

that Pb speciation, and phases formed are closely balanced and strongly influenced by the environmental conditions.

These findings also enable an estimate of the solubility product K_{sp}(plumbojar) of pure plumbojarosite by considering the dissolution reaction:

$$Pb_{0.5}Fe_3(SO_4)_2(OH)_6 + 6H^+_{(aq)} \leftrightarrow 0.5Pb^{2+}_{(aq)} + 3Fe^{3+}_{(aq)} + 2SO_4{}^{2-}_{(aq)} + 6H_2O_{(l)} \quad (7)$$

with

$$\Delta G^{\circ}_{dissolution} = \left(\sum_i v_i \cdot G^{\circ}_f(i)\right) - G^{\circ}_f(\text{plumbojar}) = -RT \cdot Ln(K_{sp}) = -2.303 \cdot RT \cdot Log(K_{sp}) \quad (8)$$

where v_i is the coefficient of the species "i" formed on the right side of reaction (7). Application of Eq. (8) then leads to $\Delta G^{\circ}_{dissolution} = 145.3 \pm 5.8$ kJ/mol, giving at 298 K: Log (K_{sp}(plumbojar)) ≈ −25.5 ± 1.0. Note that this value is significantly more negative than the one (−11.42) calculated by Gaboreau and Vieillard (2004) from the data reported by Kashkay et al. (1975) and treating that sample as stoichiometric. This difference might explain for example the observation of plumbojarosite in systems where its formation was not initially anticipated, for example in hydrometallurgical processes. It is also possible to estimate the evolution of the solubility product with temperature. This is indeed possible, assuming a constant ΔC_p for the dissolution reaction in the temperature range considered, by splitting the $\Delta G^{\circ}_{dissolution}$ into its enthalpy and entropy terms: $\Delta G^{\circ}_{dissolution} = \Delta H^{\circ}_{dissolution} - T \cdot \Delta S^{\circ}_{dissolution}$, where $\Delta H^{\circ}_{dissolution} = 79.1 \pm 9.8$ kJ/mol and $\Delta S^{\circ}_{dissolution} = -750.3 \pm 23.0$ J/(mol K) (this last uncertainty being mostly due to the high uncertainty on the absolute entropy of Fe^{3+} aqueous ions ($S^{\circ}(Fe^{3+}_{aq}) = -280.0 \pm 13.0$ J/(mol K), Robie and Hemingway, 1995). Examples of such estimated solubility products are given in Table 3 for the range 5–45 °C (278–318 K).

4. CONCLUSION

The enthalpy of formation from the elements of a Pb-jarosite sample was determined by oxide melt drop solution calorimetry. This measure is the first direct measurement of the heat of formation for a lead-containing jarosite. The thermochemical behavior of this sample, a nonstoichiometric member of the hydronium jarosite–plumbojarosite series, was then compared to that of the corresponding end-members and thermochemical data were derived as a first approximation for the formation from the elements of ideal plumbojarosite. The existence of a negative enthalpy of mixing in the plumbojarosite–hydroxyjarosite solid solution was suggested, probably related to a nonrandom organization of Pb^{2+} ions within the jarosite structure. The data should prove useful for the (re)evaluation of phase diagrams and for other thermochemical-geochemical calculations. Examples of the calculation of Eh–pH diagram and solubility product were given.

ACKNOWLEDGMENTS

This work was funded by the US Department of Energy (Grant DEFG0397SF14749) to A. Navrotsky and through the UK Engineering and Physical Sciences Research Council (EPSRC) studentship award (No. 309778) to A.M.L. Smith. We thank A.S. Wills for the GSAS refinement of the original synthetic Pb-jarosite, C. Jones and A. Ball for help with SEM analysis and photography, G. Jones and V. Din for assistance with geochemical analysis, and I. Wood for expert help with the XRD analysis.

REFERENCES

Ardau C., Frau F., Nieddu G. and Fanfani L. (2007) Field evidences on release/removal of arsenic by hydrotalcite-like compounds in mining waters. The example of Baccu Locci Mine (Sardinia, Italy). In *Water in Mining Environments* (eds. R. Cidu and F. Frau), pp. 385–389. Water in Mining Environments. Mako Edizioni, Cagliari, Sardinia.

Bale C. W., Chartrand P., Degterov S. A., Eriksson G., Hack K., Ben Mahfoud R., Melancon J., Pelton A. D. and Petersen S. (2002) FactSage thermochemical software and databases. *Calphad* **26**(2), 189–228.

Barin I. (1989) Thermochemical data of pure substances (eds. H. F. Ebel and C. D. Brenzinger). VCH Verlagsgesellschaft, Weinheim.

Barin I. (1993) *Thermochemical Data of Pure Substances*, second ed. VCH Verlags Gesellschaft, Weinheim.

Baron D. and Palmer C. D. (1996a) Solubility of jarosite at 4–35 °C. *Geochim. Cosmochim. Acta* **60**, 185–195.

Baron D. and Palmer C. D. (1996b) Solubility of $KFe_3(CrO_4)_2(OH)_6$ at 4 to 35 °C. *Geochim. Cosmochim. Acta* **60**(20), 3815–3824.

Baron D. and Palmer C. D. (2002) Solid-solution aqueous-solution reaction between jarosite ($KFe_3(SO_4)_2(OH)_6$) and its chromate analog. *Geochim. Cosmochim. Acta* **66**(16), 2841–2853.

Brunauer S., Emmett P. H. and Teller E. (1938) Adsorption of gases in multimolecular layers. *Am. Chem. Soc. J.* **60**, 309–319.

Drouet C., Baron D. and Navrotsky A. (2003) On the thermochemistry of the solid solution between jarosite and its chromate analog. *Am. Mineral.* **88**, 1949–1954.

Drouet C. and Navrotsky A. (2003) Synthesis, characterisation and thermochemistry of K–Na–H_3O jarosites. *Geochim. Cosmochim. Acta* **67**(11), 2063–2076.

Dutrizac J. E. (1991) The precipitation of lead jarosite from chloride media. *Hydrometallurgy* **26**(3), 327–346.

Dutrizac J. E. and Chen T. T. (1981) The synthesis of mercury jarosite and the mercury concentration in jarosite-family minerals. *Can. Mineral.* **19**(4), 559–569.

Dutrizac J. E. and Chen T. T. (2000) The behaviour of gallium during jarosite precipitation. *Can. Metall. Q.* **39**(1), 1–14.

Dutrizac J. E. and Chen T. T. (2003) Syntesis and properties of V^{3+} analogues of jarosite-group minerals. *Can. Mineral.* **41**, 479–488.

Dutrizac J. E., Dinardo O. and Kaiman S. (1980) Factors affecting lead jarosite formation. *Hydrometallurgy* **5**(4), 305–324.

Dutrizac J. E. and Jambor J. L. (1985) Formation and characterization of argentojarosite and plumbojarosite and their relevance to metallurgical processing. In *Applied Mineralogy* (eds. W. C. Park, D. M. Hausen and R. D. Hagni). Warrendale, Pennsylvania, pp. 507–530.

Dutrizac J. E. and Jambor J. L. (1987) The behavior of arsenic during jarosite precipitation: arsenic precipitation at 97 degree from sulfate or chloride media. *Can. Metall. Q.* **26**, 91–101.

Dutrizac J. E. and Jambor J. L. (2000) Jarosite and their application in hydrometallurgy. In *Sulfate Minerals: Crystallography, Geochemistry and Environmental Significance*, vol. 40 (eds. C. N. Alpers and J. L. Jambor). Mineralogical Society of America, pp. 405–452.

Dutrizac J. E., Hardy D. J. and Chen T. T. (1996) The behaviour of cadmium during jarosite precipitation. *Hydrometallurgy* **41**, 269–285.

Dutrizac J. E. and Kaiman S. (1976) Synthesis and properties of jarosite-type compounds. *Can. Mineral.* **14**, 151–158.

Forray F. L., Drouet C. and Navrotsky A. (2005) Thermochemistry of yavapaiite $KFe(SO_4)_2$: formation and decomposition. *Geochim. Cosmochim. Acta* **69**(8), 2133–2140.

Frau F., Ardau C. and Asunis I. (2007) Geochemistry of lead at the old mine area of Baccu Locci (South-East Sardinia, Italy). In *Water in Mining Environments* (eds. R. Cidu and F. Frau). Mako Edizioni, Cagliari, Sardinia, pp. 427–432.

Frau F., Ardaua C. and Fanfania L. (2009) Environmental geochemistry and mineralogy of lead at the old mine area of Baccu Locci (South-East Sardinia, Italy). *J. Geochem. Explor.* **100**, 105–115.

Frost R. L., Wills R.-A., Weier M. L., Musumeci A. W. and Martens W. (2005) Thermal decomposition of natural and synthetic plumbojarosites: importance in 'archeochemistry'. *Thermochim. Acta* **432**(1), 30–35.

Gaboreau S. and Vieillard P. (2004) Prediction of Gibbs free energies of formation of minerals of the alunite supergroup. *Geochim. Cosmochim. Acta* **68**(16), 3307–3316.

Hendricks S. B. (1937) The crystal structure of alunite and the jarosite. *Am. Mineral.* **22**, 773–784.

Hochella M. F., Moore J. N., Golla U. and Putnis A. (1999) A TEM study of samples from acid mine drainage systems: metal–mineral association with implications for transport. *Geochim. Cosmochim. Acta* **63**, 3395–3406.

Hochella J., Michael F., Moore J. N., Putnis C. V., Putnis A., Kasama T. and Eberl D. D. (2005) Direct observation of heavy metal–mineral association from the clark fork river superfund complex: implications for metal transport and bioavailability. *Geochim. Cosmochim. Acta* **69**(7), 1651–1663.

Hudson-Edwards K. A., Schell C. and Macklin M. G. (1999) Mineralogy and geochemistry of alluvium contaminated by metal mining in the Rio Tinto area, Southwest Spain. *Appl. Geochem.* **14**, 1015–1030.

Jambor J. L. and Dutrizac J. E. (1983) Beaverite–plumbojarosite solid solutions. *Can. Mineral.* **21**(1), 101–113.

Kashkay C. M., Borovskaya Y. B. and Babazade M. A. (1975) Determination of deltaG°f 298 of synthetic jarosite and its sulfate analogues. *Geokhimiya* **5**, 778–784.

Knopf A. (1915) Plumbojarosite and other lead-ferric sulfates (vegasite) from the Yellow Pine district, Nevada. *J. Washington Acad. Sci.* **5**, 497–503.

Kubisz J. (1970) Studies on synthetic alkali-hydronium jarosite. I. Synthesis of jarosite and natrojarosite. *Mineral. Pol.* **1**, 47–57.

Kubisz J. (1971) Studies on synthetic alkali-hydronium jarosites. II. Thermal investigations. *Mineral. Pol.* **2**, 51–59.

Lengauer C. L., Giester G. and Irran E. (1994) $KCr_3(SO_4)_2(OH)_6$: synthesis, characterization, powder diffraction data, and structure refinement by the Rietveld technique and a compilation of alunite-type compounds. *Powder Diffr.* **9**(4), 265–271.

Leybourne M. I., Peter J. M., Layton-Matthews D., Volesky J. and Boyle D. R. (2006) Mobility and fractionation of rare earth elements during supergene weathering and gossan formation and chemical modification of massive sulfide gossan. *Geochim. Cosmochim. Acta* **70**, 1097–1112.

Majzlan J., Navrotsky A. and Neil J. M. (2002) Energetics of anhydrite, barite, celestine, and anglesite: a high-temperature and differential scanning calorimetry study. *Geochim. Cosmochim. Acta* **66**(10), 1839–1850.

Majzlan J., Navrotsky A., Stevens R., Boerio-Goates J., Woodfield B. F., Burns P. C., Crawford M. K. and Amos T. G. (2004) Thermodynamic properties, low-temperature heat capacity anomalies, and single crystal X-ray refinement of hydronium jarosite, $(H_3O)Fe_3(OH)_6(SO_4)_2$. *Phys. Chem. Miner.* **31**, 518–531.

Mumme W. G. and Scott T. R. (1966) The relationship between basic ferric sulfate and plumbojarosite. *Am. Mineral.* **51**, 443–453.

Navrotsky A. (1977) Progress and new directions in high temperature calorimetry. *Phys. Chem. Miner.* **2**, 89–104.

Navrotsky A. (1997) Progress and new directions in high temperature calorimetry revisited. *Phys. Chem. Miner.* **24**, 222–241.

Ostergren J. D., Brown G. E. J., Parks G. A. and Tingle T. N. (1999) Quantitative speciation of lead in selected mine tailings from Leadville. CO. *Environ. Sci. Technol.* **33**, 1627–1636.

Özacar M., Alp A. and Aydin A. O. (2000) Kinetics of thermal decomposition of plumbo-jarosite. *J. Therm. Anal. Calorim.* **59**, 869–875.

Patiño F., Viñals J., Roca A. and Núñez C. (1994) Alkaline decomposition–cyanidation kinetics of argentian plumbojarosite. *Hydrometallurgy* **34**(3), 279–291.

Powers D. A., Rossman G. R., Schugar H. J. and Gray H. B. (1975) Magnetic behavior and infrared spectra of jarosite, basic iron sulfate, and their chromate analogs. *J. Solid State Chem.* **13**(1–2), 1–13.

Ripmeester J. A., Ratcliffe C. I., Dutrizac J. E. and Jambor J. L. (1986) Hydronium ion in the alunite–jarosite group. *Can. Mineral.* **24**(3), 435–447.

Robie R. A. and Hemingway B. S. (1995) *Thermodynamic properties of minerals and related substances at 298.15 K and 1 Bar (10^5 Pascals) pressure and at higher temperatures*, pp. 461. US Geological Survey.

Sasaki K. and Konno H. (2000) Morphology of jarosite-group compounds precipitated from biologically and chemically oxidized Fe ions. *Can. Mineral.* **38**, 45–56.

Serna C. J., Cortina C. P. and Garcia Ramos J. V. (1986) Infrared and Raman study of alunite–jarosite compounds. *Spectrochim. Acta A Mol. Spectrosc.* **42**(6), 729–734.

Smith A. M. L., Dubbin W. E., Wright K. and Hudson-Edwards K. A. (2006) Dissolution of lead- and lead-arsenic-jarosites at pH 2 and 8 and 20 °C: insights from batch experiments. *Chem. Geol.* **229**(4), 344–361.

Stoffregen R. E. (1993) Stability of jarosite and natrojarosite at 150–250 °C. *Geochim. Cosmochim. Acta* **57**, 2417–2429.